High-Efficiency Visible-Light-Driven Ag3PO4/AgI Photocatalysts: Z-Scheme Photocatalytic Mechanism for Their Enhanced Photocatalytic Activity

ARTICLE *in* THE JOURNAL OF PHYSICAL CHEMISTRY C · AUGUST 2013

Impact Factor: 4.77 · DOI: 10.1021/jp406508y

4 AUTHORS, INCLUDING:

Zhihong Chen
South China University of Technology
5 PUBLICATIONS **91** CITATIONS
SEE PROFILE

Zzg Zhengguo Zhang
South China University of Technology
64 PUBLICATIONS **1,045** CITATIONS
SEE PROFILE

Xiaoming Fang
South China University of Technology
53 PUBLICATIONS **1,498** CITATIONS
SEE PROFILE

THE JOURNAL OF PHYSICAL CHEMISTRY C

Article

pubs.acs.org/JPCC

High-Efficiency Visible-Light-Driven Ag_3PO_4/AgI Photocatalysts: Z-Scheme Photocatalytic Mechanism for Their Enhanced Photocatalytic Activity

Zhihong Chen, Weilin Wang, Zhengguo Zhang, and Xiaoming Fang*

Key Laboratory of Enhanced Heat Transfer and Energy Conservation, the Ministry of Education, School of Chemistry and Chemical Engineering, South China University of Technology, Guangzhou 510640, China

ABSTRACT: High-efficiency visible-light-driven Ag_3PO_4/AgI photocatalysts with different mole fractions of AgI have been synthesized via an in-situ anion-exchange method and characterized by X-ray diffraction (XRD), scanning electron microscopy (SEM), energy-dispersive spectroscopy (EDS), and UV−vis diffuse reflectance spectroscopy (DRS). Under visible light (>420 nm), the Ag_3PO_4/AgI photocatalysts exhibit enhanced photocatalytic activity compared to pure Ag_3PO_4 or AgI for the degradation of methyl orange and phenol, and the highest activity is reached by the Ag_3PO_4/AgI hybrid photocatalyst with 20% of AgI. The quenching effects of different scavengers suggest that the reactive h^+ and $O_2^{\bullet-}$ play the major role in the MO degradation. Detailed X-ray photoelectron spectroscopy (XPS) and transmission electron microscopy (TEM) analysis reveals that Ag nanoparticles (NPs) form on the surface of Ag_3PO_4/AgI in the early stage of the photocatalytic oxidation process, thus leading to the transformation from Ag_3PO_4/AgI to Ag_3PO_4/AgI@Ag. The excellent photocatalytic activity of the Ag_3PO_4/AgI photocatalysts can be ascribed to the efficient separation of photogenerated electron−hole pairs through a Z-scheme system composed of Ag_3PO_4, Ag, and AgI, in which the Ag nanoparticles acted as the charge transmission bridge. The Ag_3PO_4/AgI hybrid remains good photocatalytic activity after five cycling runs.

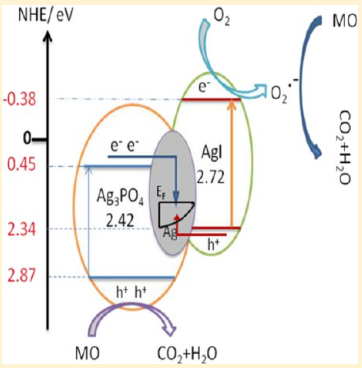

INTRODUCTION

Photocatalytic H_2 productions from water splitting and degradation of pollutants over semiconductors under solar irradiation have attracted more and more attention due to its potential as one of clean, low-cost, and environmentally friendly strategies to solve the energy crisis and environmental contamination.[1,2] Developing high-efficiency semiconductor photocatalysts is essential to transform the two technologies into practical applications. Since the discovery of photoelectrochemical splitting of water from TiO_2 electrodes by Honda,[3] TiO_2 has been the subject of extensive investigation due to its high efficiency, low cost, nontoxicity, and high stability over the past three decades.[4−6] However, TiO_2 can only absorb the UV light, which accounts for only 4% of the total sunlight and thus greatly restricts its practical applications under solar light. Therefore, researches on high-efficiency visible-light-driven photocatalysts have become hot issues in the photocatalysis field.

Recently, Ag-based photocatalysts have been developed as efficient photocatalysts on degradation of pollutants, such as AgX (X = Cl, Br, and I),[7−9] Ag_2O,[10] and Ag_2CO_3.[11] Among those Ag-based semiconductors, Ag_3PO_4 has an indirect band gap of 2.36 eV and a direct band gap of 2.43 eV, which make it show potential for use as a visible-light-driven photocatalyst. In 2010, Ye et al.[12] reported the new use of Ag_3PO_4 in the O_2 evolution from photooxidation of water and photodecomposition of organic dye under visible light, in which remarkable quantum efficiency up to 90% at wavelengths longer than 420 nm was achieved. The further investigation on the origin of photocatalytic activation of Ag_3PO_4 showed that both the large dispersion of conduction band and the inductive effect of PO_4^{3-} contributed to the electron−hole pairs separation for Ag_3PO_4.[13] Moreover, the photocatalytic activity of Ag_3PO_4 can be further improved through the modulation on the shape, morphology, and crystal face of Ag_3PO_4 crystals.[14−19] However, there are still some inherent shortcomings in Ag_3PO_4: the conduction band potential of Ag_3PO_4 (0.45 eV vs NHE) is more positive than that of H_2−H^+, which limits its application in hydrogen production from water splitting; Ag particles usually generate from the photodecomposition of Ag_3PO_4 under light irradiation; the dissolution of Ag_3PO_4 in water should be taken into consideration during the photocatalytic process. Therefore, it is necessary to develop novel Ag_3PO_4-based photocatalysts with improved photocatalytic activity and stability.

More recently, several kinds of materials have been used to cooperate with Ag_3PO_4 to generate hybrid photocatalysts, which include wide-bandgap semiconductors (TiO_2, ZnO, SnO_2, etc.),[20−25] narrow-bandgap semiconductors ($BiMoO_4$ and g-C_3N_4),[26,27] and carbon materials (oxidized graphene, graphene, and carbon quantum dots).[28−32] The Ag_3PO_4-based hybrid with a wide-bandgap semiconductor suffers from the low

Received: July 2, 2013
Revised: August 27, 2013
Published: August 29, 2013

dx.doi.org/10.1021/jp406508y | J. Phys. Chem. C 2013, 117, 19346−19352

visible light activity of the wide-bandgap component. Although the hybrids with narrow-bandgap semiconductors can improve the optical absorption property and facilitate the separation of photogenerated electron−hole pairs, the obtained heterojunction structure results in the remaining electrons and holes with less reducibility and oxidability. The combination of Ag_3PO_4 with carbon materials can facilitate electron transport and restrain hole−electron recombination due to the excellent electrical conductivity of carbon materials. However, the carbon materials have a more negative conduction band potential than that of Ag_3PO_4, which hinders the photogenerated electron transfer from Ag_3PO_4 to the carbon materials. In 2011, Ye et al.[33] demonstrated Ag_3PO_4/AgX (X = Cl, Br, and I) core/shell heterocrystals showed superior photocatalytic activity over single Ag_3PO_4. And in 2012, Cao et al.[34] reported that the photocatalytic activity of Ag_3PO_4/AgBr was higher than those of Ag_3PO_4 and AgBr. In the current work, with the purpose of developing a novel kind of Ag_3PO_4-based hybrid photocatalysts with high activity as well as good stability, AgI with a more negative conduction band than AgBr was chosen as the component to combine with Ag_3PO_4, thus providing the obtained Ag_3PO_4/AgI hybrid photocatalyst with a higher driving force between the two components. First, Ag_3PO_4/AgI hybrids with different mole fractions of AgI were prepared by an in-situ ion-exchange method, followed by the characterizations by XRD, SEM, TEM, and UV−vis spectrometer. Second, the photocatalytic activities of the Ag_3PO_4/AgI hybrids with different mole fractions of AgI were evaluated by decomposing methyl orange (MO) and phenol (PhOH) under visible light (>420 nm), and the optimal mole fraction of AgI was determined. Third, the photocatalytic mechanism of the Ag_3PO_4/AgI hybrid photocatalyst was investigated through several reactive species trapping and hydroxyl radical quantification experiments, and the efficient separation of photogenerated electron−hole pairs through a Z-scheme system composed of Ag_3PO_4, Ag, and AgI was elucidated. Finally, the stability of the Ag_3PO_4/AgI hybrid photocatalyst was examined.

EXPERIMENTAL SECTION

Preparation of Ag_3PO_4/AgI Photocatalyst. In a typical process, 2.4 g of silver nitrate and 1.152 g of sodium dihydrogen phosphate were dissolved in 40 mL of deionized water and then the obtained sodium dihydrogen phosphate solution was dropped in the silver nitrate solution under mild stirring. After stirring for 1 h, the precipitates was washed by deionized water for 3 times, collected by centrifugation, and dried at 50 °C for 24 h to obtain Ag_3PO_4.

Ag_3PO_4/AgI hybrid photocatalysts were prepared through an in-situ anion-exchange method in a dark condition at room temperature. 1 g of Ag_3PO_4 was dispersed in 50 mL of deionized water by ultrasound, and then different amounts of sodium iodide dissolved in 20 mL of deionized water were dropped in the Ag_3PO_4 dispersion in which the theoretical molar ratios of I/P were controlled to be 10%, 20%, and 30%. After stirring for 6 h vigorously, the precipitates were collected, washed with deionized water for three times, and dried at 50 °C for 24 h. The final samples were denoted as Ag_3PO_4/AgI-10%, Ag_3PO_4/AgI-20%, and Ag_3PO_4/AgI-30%, respectively.

Characterizations. Powder X-ray diffraction (XRD) measurements were performed on the D/max-IIIA instrument using Cu Kα radiation at a scanning rate of 0.02 deg/s. The morphologies of the samples were observed with a scanning electron microscope (S-3700N), and their energy-dispersive spectroscopy (EDS) was observed using an Oxford instruments INCA 300 detector. Diffuse reflectance spectra (DRS) of the samples were obtained by a Shimadzu U-3010 spectrophotometer equipped with an integrating sphere assembly. TEM images were obtained by a PHILIPS TECNAI-10 field emission electron microscope. X-ray photoelectron spectroscopy (XPS) measurements were carried out on a THETA Prode spectrometer, and the spectra were calibrated to the C 1s peak at 284.8 eV.

Evaluation of Photocatalytic Activities and Detection of Active Oxygen Species. The photocatalytic activities of the samples were evaluated by degrading MO or PhOH under visible light irradiation. The visible light was obtained from a 500 W Xe lamp with a 420 nm cutoff filter. In each experiment, 0.1 g of photocatalyst was dispersed in 50 mL of deionized water, followed by adding 50 mL of MO or PhOH solution (20 mg/L). Prior to illumination, the suspension was stirred for 30 min to reach the desorbance−absorbance equilibrium. At irradiation time intervals of 3 min, 5 mL of the suspension was collected and then centrifuged (8000 rpm, 30 min) to remove the photocatalyst particles. The upper clear liquid was analyzed by a Shimadzu UV-2050 spectrophotometer to record the maximum absorption band (462 nm for MO and 270 nm for PhOH).

In order to detect the active species during the photocatalytic reaction, isopropanol (IPA), ammonium oxalate (AO), and benzoquinone (BQ) were added into the MO solution dispersed with the Ag_3PO_4/AgI hybrid photocatalyst to capture hydroxyl radicals ($^{\bullet}OH$), holes (h^+), and the superoxide radicals ($O_2^{\bullet-}$), respectively, followed by the photocatalytic activity test. In addition, the aqueous solution containing 10 mM NaOH and 3 mM terephthalic acid ($C_8H_6O_4$, TA) was used to test the existence of $^{\bullet}OH$ by the fluorescent method due to the generation of the luminescent 2-hydroxyterephthalic acid (TAOH) by the reaction between $^{\bullet}OH$ and TA . A fluorescence spectrophotometer (F-4500) was used to measure the fluorescence signal of the TAOH.

RESULTS AND DISCUSSION

Structural, Morphological and Optical Absorption Properties of Ag_3PO_4/AgI. Figure 1 displays the XRD patterns of the Ag_3PO_4/AgI hybrid photocatalysts with

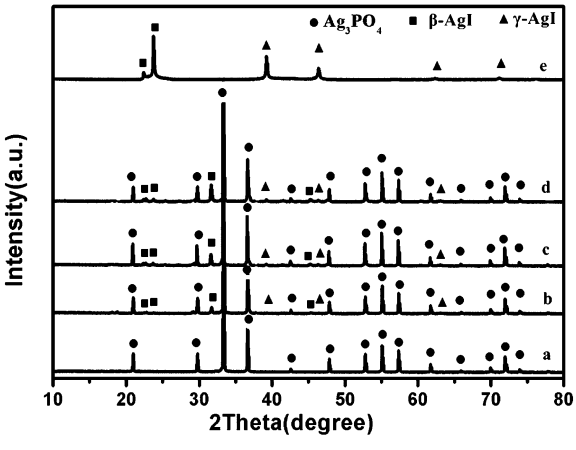

Figure 1. XRD patterns of Ag_3PO_4 (a), Ag_3PO_4/AgI-10% (b), Ag_3PO_4/AgI-20% (c), Ag_3PO_4/AgI-30% (d), and AgI (e).

dx.doi.org/10.1021/jp406508y | J. Phys. Chem. C 2013, 117, 19346−19352

different mole ratios of AgI, together with those of AgI and Ag_3PO_4. It is observed that Ag_3PO_4 is cubic phase (JCPDS No. 06-0505) (Figure 1a), while AgI is a mixed crystal of hexagonal β-AgI (no. 85-0801) and cubic γ-AgI (no. 09-0399) (Figure 1e). The Ag_3PO_4/AgI hybrids (Figure 1b–d) exhibit a coexistence of both AgI and Ag_3PO_4 phases. Furthermore, the intensities of the diffraction peaks of AgI increase with the mole ratio of AgI in the hybrids, whereas those of Ag_3PO_4 decreased simultaneously. The diffraction peaks of AgI in the Ag_3PO_4/AgI hybrids are slightly different from those of the AgI sample due to the different growth conditions.[35]

Figure 2 displays the SEM images of Ag_3PO_4 and the Ag_3PO_4/AgI hybrids with different mole ratios of AgI. The as-

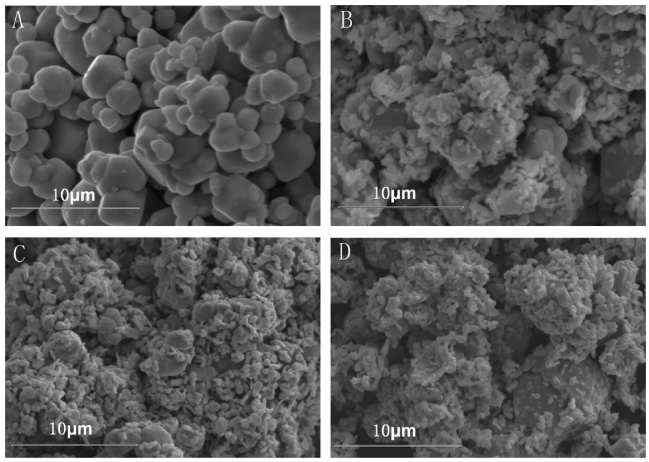

Figure 2. SEM images Ag_3PO_4(A), Ag_3PO_4/AgI-10% (B), Ag_3PO_4/AgI-20% (C), and Ag_3PO_4/AgI-30% (D).

prepared Ag_3PO_4 particles have an irregular morphology with ca. 0.2–2 μm in size (Figure 2A). After the ion-exchange reaction between Ag_3PO_4 and NaI, small AgI particles have been formed on the surfaces of the Ag_3PO_4 particles, and the amount of the AgI particles increases with the mole ratio of AgI (Figure 2B–D).

The EDS results of Ag_3PO_4, Ag_3PO_4/AgI-10%, Ag_3PO_4/AgI-20%, Ag_3PO_4/AgI-30%, and AgI are listed in Table 1. The pure

Table 1. EDS Results of Ag_3PO_4, Ag_3PO_4/AgI-10%, Ag_3PO_4/AgI-20%, Ag_3PO_4/AgI-30%, and AgI

	atom content (at. %)			
catalyst	Ag	P	O	I
Ag_3PO_4	32.31	10.82	56.87	0
Ag_3PO_4/AgI-10%	35.44	11.90	51.97	0.69
Ag_3PO_4/AgI-20%	36.09	11.46	51.02	1.43
Ag_3PO_4/AgI-30%	37.57	11.61	48.38	2.44
AgI	50.18	0	0	48.82

Ag_3PO_4 sample is composed of Ag, P, and O elements, whereas the Ag_3PO_4/AgI hybrids are composed of Ag, P, I, and O elements, further confirming the existence of AgI. The atom content of I increases with the mole ratio of AgI in the Ag_3PO_4/AgI hybrids, which is accordance with the SEM and XRD data. For all the hybrid samples, it is found that the atom content of Ag is equal to the sum of the atom content of I and that of the trinary-P, implying that no Ag nanoparticles formed in the hybrids. In addition, no other impurity is found in the hybrid photocatalysts.

Figure 3A displays the UV–vis diffuse reflectance spectra of the Ag_3PO_4/AgI hybrids with different mole ratios of AgI, together with those of Ag_3PO_4 and AgI. Pure AgI has an absorption edge at about 450 nm, while pure Ag_3PO_4 has a broader absorption in the visible region with an absorption edge at about 530 nm. The Ag_3PO_4/AgI hybrids exhibit the two absorption edges at both 450 and 530 nm, implying a combination of the optical absorption property of AgI with that of Ag_3PO_4.[33] For the Ag_3PO_4/AgI hybrids, as the mole ratio of I/P is increased, the absorption edge at about 450 nm for AgI increases whereas that at 530 nm for Ag_3PO_4 decreases simultaneously.

According to the plot of $(ahv)^{2/n}$ versus energy, as shown in Figure 3B, the band gap energies (E_g) of Ag_3PO_4 and AgI have been calculated to be 2.42 and 2.72 eV, respectively. The band structure of Ag_3PO_4/AgI can be estimated according to the empirical equations

$$E_{VB} = \chi - E^e + 0.5E_g \quad (1)$$

$$E_{CB} = E_{VB} - E_g \quad (2)$$

where E_{VB} is the valence band edge potential, χ is the electronegativity of the semiconductor, which is the geometric mean of the electronegativity of the constituent atoms, and E^e is the energy of free electrons on the hydrogen scale (about 4.5 eV vs NHE). The χ values for AgI and Ag_3PO_4 are 5.48 and 6.16 eV, respectively. Thus, the E_{VB} of AgI and Ag_3PO_4 have been calculated to be 2.34 and 2.87 eV vs NHE, and their corresponding E_{CB} are −0.38 and 0.45 eV vs NHE, respectively.

Photocatalytic Activity of Ag_3PO_4/AgI. Figure 4A displays the photodegradation of MO as a function of irradiation time over different photocatalysts. Based on the blank (in the absence of any catalyst) experiment, the self-photolysis of MO under visible light irradiation can be ignored. It can be seen from Figure 4A that all the Ag_3PO_4/AgI hybrids exhibit higher photocatalytic activities than pure Ag_3PO_4 or AgI. Under the visible light irradiation for 18 min, 93.6%, 96.9%, and 91.4% of MO has been degraded over Ag_3PO_4/AgI-10%, Ag_3PO_4/AgI-20%, and Ag_3PO_4/AgI-30%, respectively. Ag_3PO_4/AgI-20% exhibits the highest photocatalytic activity. As the mole fraction of AgI is increased from 20% to 30%, a decrease in the photocatalytic activity of Ag_3PO_4/AgI is observed. The probable reason for this decrease is that more AgI particles have been formed on the surfaces of the Ag_3PO_4 particles as the mole ratio of AgI is further increased, which decreases the light absorbance of Ag_3PO_4 and isolates the direct contact between Ag_3PO_4 and MO molecules. Furthermore, phenol, a substance without absorbing visible light, has been used to verify the visible light photocatalytic property of the as-prepared samples under visible light (>420 nm), and the obtained results are illustrated in Figure 4B. All the Ag_3PO_4/AgI hybrids and pure Ag_3PO_4 exhibit excellent photocatalytic activities on the degradation of PhOH under visible light, which further confirms their inherent visible light photocatalytic properties.

In addition, a comparison on the photocatalytic activity between Ag_3PO_4/AgI-20% (0.1 g) and a mixture of AgI (0.07 g) and Ag_3PO_4 (0.093 g) has been conducted. The mole ratios of AgI and Ag_3PO_4 in the two samples are the same. It can be clearly seen from Figure 5 that the photocatalytic activity of Ag_3PO_4/AgI-20% is much higher than that of the mixture of AgI and Ag_3PO_4, implying that the efficient charge separation occurs in Ag_3PO_4/AgI-20% rather than in the mixture.

dx.doi.org/10.1021/jp406508y | J. Phys. Chem. C 2013, 117, 19346–19352

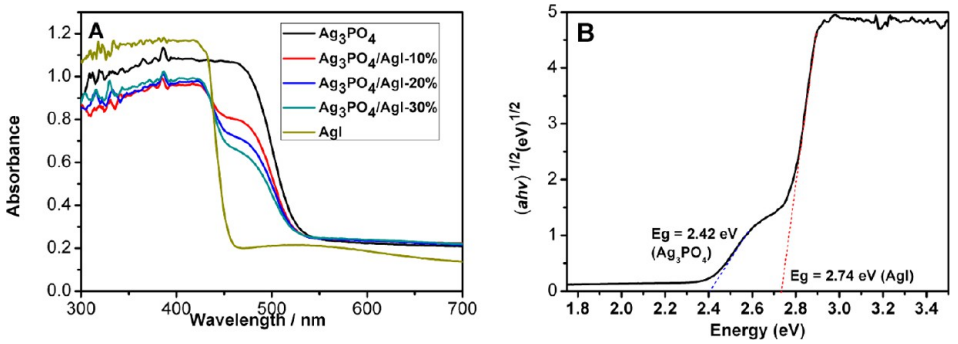

Figure 3. (A) UV−vis diffuse reflectance spectra of Ag_3PO_4, Ag_3PO_4/AgI-10%, Ag_3PO_4/AgI-20%, Ag_3PO_4/AgI-30%, and AgI. (B) Plot of $(\alpha h\nu)^{1/2}$ versus energy $(h\nu)$ for Ag_3PO_4/AgI-20%.

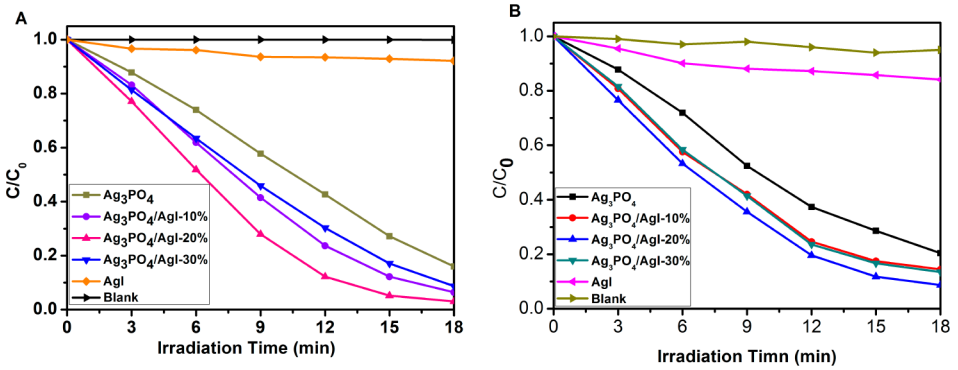

Figure 4. Photocatalytic activities of Ag_3PO_4, AgI, and the Ag_3PO_4/AgI hybrids on the degradation of MO (A) and PhOH (B) under visible light irradiation (>420 nm).

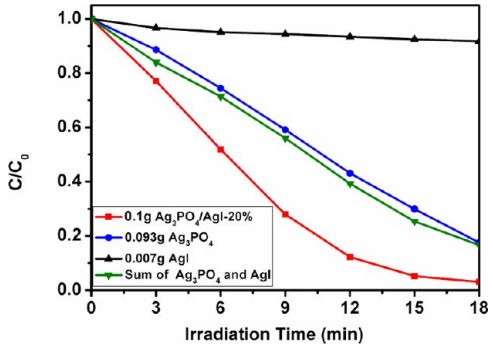

Figure 5. Comparison on the photocatalytic activity of Ag_3PO_4/AgI-20% (0.1 g) with that of the mixture of Ag_3PO_4 and AgI with the same mole and weight fraction of AgI (0.093 g of Ag_3PO_4 + 0.07 g of AgI) for the degradation of MO under visible light irradiation (>420 nm).

Photocatalytic Mechanism of Ag_3PO_4/AgI. In the photocatalytic oxidation (PCO) process, a series of reactive oxygen species, such as h^+, $^{\bullet}OH$, or $O_2^{\bullet-}$, are supposed to be involved. In order to investigate why the Ag_3PO_4/AgI hybrid is so efficient for the degradation of MO, we conducted the reactive species trapping and hydroxyl radical quantification experiments. Isopropanol (IPA), ammonium oxalate (AO), and benzoquinone (BQ) acted as the scavengers for $^{\bullet}OH$, h^+, and $O_2^{\bullet-}$ were introduced into the PCO process, respectively. Figure 6 shows the photocatalytic activities of Ag_3PO_4/AgI-20% on the degradation of MO in presence of different scavengers. It can be seen that the addition of IPA in the MO solution has little effect on the photocatalytic activity of Ag_3PO_4/AgI-20%, suggesting that $^{\bullet}OH$ does not play a key role for the degradation of MO. On the contrary, the photocatalytic degradation of MO is obviously inhibited after the addition

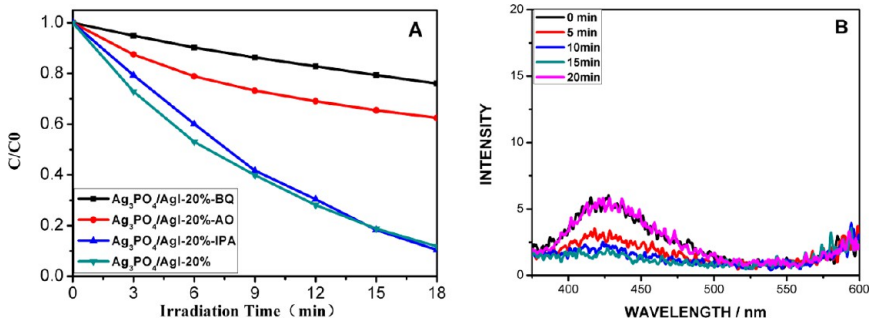

Figure 6. Photocatalytic activities of Ag_3PO_4/AgI-20% on the degradation of MO in presence of different scavengers under visible light irradiation (>420 nm) (A) and $^{\bullet}OH$ trapping PL spectra in TA solution of the used Ag_3PO_4/AgI-20% under visible light irradiation (>420 nm).

dx.doi.org/10.1021/jp406508y | J. Phys. Chem. C 2013, 117, 19346−19352

of AO and BQ. On the basis of these results, it can be concluded that h^+ and $O_2^{\bullet-}$ are the main oxygen active species for Ag_3PO_4/AgI-20% in the MO solution under visible light irradiation. Since the E_{CB} potential of AgI is more negative than $E_0(O_2/O_2^{\bullet-})$ (−0.046 eV vs NHE), the electrons left on the E_{CB} of AgI reduce O_2 to $O_2^{\bullet-}$ through one-electron reducing reaction. The results from the hydroxyl radical quantification experiments (Figure 6B) further confirm that $^{\bullet}OH$ is not the main oxygen active species in the PCO process.

In order to further elucidate the photocatalytic mechanism of the Ag_3PO_4/AgI hybrid photocatalyst, Ag_3PO_4/AgI-20% before and after 1 and 5 recycling runs have been characterized by EDS, and the obtained results are listed in Table 2. It is found

Table 2. EDS Results of 20% AgI/Ag_3PO_4 and the 20% AgI/Ag_3PO_4 after 1 and 5 Recycling Runs

	atom content (at. %)			
catalyst	Ag	P	O	I
Ag_3PO_4/AgI-20%	36.09	11.46	51.02	1.43
Ag_3PO_4/AgI-20% after 1 run	34.22	10.34	54.07	1.37
Ag_3PO_4/AgI-20% after 5 runs	36.94	10.72	50.92	1.42

that the atom content of Ag is higher than the sum of the atom content of I and that of trinary-P for the two used samples, implying the existence of metallic Ag. Figure 7 shows the TEM images of Ag_3PO_4/AgI-20% before and after 1 recycling run. Clearly, no Ag NPs is found on the fresh Ag_3PO_4/AgI-20% sample, but there are some on the surface of the used one. Furthermore, the surface element composition and chemical state for the used Ag_3PO_4/AgI-20% sample have been analyzed by XPS, and the obtained results are shown in Figure 8. The peaks at 619.2 and 632.1 eV can be attributed to I 3d of AgI, while the peak at 132.3 eV belongs to P 2p of Ag_3PO_4 (Figure 8A). As shown in Figure 8B, the Ag 3d peaks have been fitted using the XPSPEAK software to separate the Ag^+ peaks and Ag^0 peaks. The weak peaks at 368.28 and 374.36 eV are attributed to Ag^0, while the strong peaks at 367.8 and 373.9 eV are assigned to Ag^+ of AgI and Ag_3PO_4.[36] The XPS results further confirm the existence of Ag NPs in the used Ag_3PO_4/AgI-20% sample. It can be inferred that the Ag nanoparticles have been formed on the surface of the Ag_3PO_4/AgI hybrid photocatalyst during the PCO process and have contact with both AgI and Ag_3PO_4, which can act as a charge transmission bridge in the hybrid catalyst.

Based on the above results, the photocatalytic mechanism of the Ag_3PO_4/AgI photocatalyst is shown in Scheme 1. Ag_3PO_4/AgI transforms to Ag_3PO_4/AgI @Ag in the early stage of the photocatalytic reaction because of the photosensition of Ag_3PO_4/AgI. The Ag NPs act as the charge transmission bridge to form the visible-light-driven Ag_3PO_4/AgI Z-scheme system. Furthermore, PO_4^{3-} ions with large negative charge in Ag_3PO_4 prefer to attract holes and repel electrons, which is in favor of the formation visible-light-driven Ag_3PO_4/AgI Z-scheme system. Under visible light irradiation, both Ag_3PO_4 and AgI are excited, and the photogenerated electrons and holes are in their conduction and valence band, respectively. There are two photogenerated electron−hole transmission channels in the visible-light-driven Z-scheme Ag_3PO_4/AgI system (internal and external transmission channels). In the internal transmission channel, the electrons in the E_{CB} of Ag_3PO_4 shift to metallic Ag due to the E_{CB} of Ag_3PO_4 is more negative than the Fermi level of metallic Ag. Simultaneously, the holes in the E_{VB} of AgI move to metallic Ag due to the E_{VB} of AgI is more positive than the Fermi level of metallic Ag and combine with the electrons here. Therefore, the internal charge transmission enhances the separation of photogenerated electron−hole pairs in the Ag_3PO_4/AgI system. In the external transmission channel, the electrons in the E_{CB} of AgI with more negative potential display strong reduction power while holes in the E_{VB} of Ag_3PO_4 show strong oxidation ability. The high reducing electron located on the CB bottom of AgI will react with molecular oxygen to form $O_2^{\bullet-}$ that can further oxidize MO. The holes located on the VB top of Ag_3PO_4 will photocatalytic oxidized MO directly due to high positive potential of the E_{VB} of Ag_3PO_4 and inductive effective of PO_4^{3-}, respectively.

Stability of Ag_3PO_4/AgI Photocatalyst. To evaluate the stability and reusability of the Ag_3PO_4/AgI hybrid photocatalyst, we carried out the additional experiments to degrade MO under visible light cycled for five times (Figure 9). The photocatalytic activity of Ag_3PO_4/AgI-20% for MO degradation is effectively maintained except for 8.6% decrease from 96.0% to 87.4% after five cycling runs, which indicates that Ag_3PO_4/AgI-20% has high stability in the PCO process under visible light. It can be drawn a conclusion that Ag_3PO_4/AgI-20% has high stability for MO degradation under visible light from the above XRD, EDS, DRS, and cycling runs results.

CONCLUSIONS

Novel high-efficiency visible-light-driven Ag_3PO_4/AgI systems have been prepared via facile precipitation-ion exchange process. The as-prepared Ag_3PO_4/AgI hybrids exhibit excellent photocatalytic activity on the degradation of MO, which is superior over those of pure Ag_3PO_4 and AgI under visible light (>420 nm). Ag NPs easily form on the surface of Ag_3PO_4/AgI

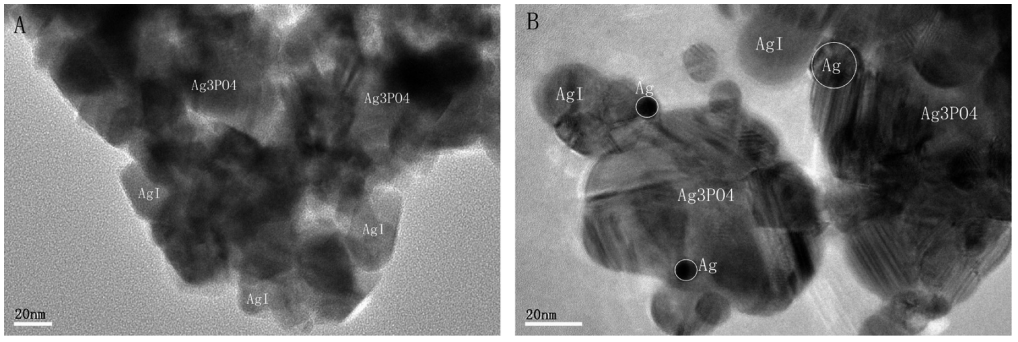

Figure 7. TEM images of Ag_3PO_4/AgI-20% before (A) and after (B) 1 recycling run.

dx.doi.org/10.1021/jp406508y | J. Phys. Chem. C 2013, 117, 19346−19352

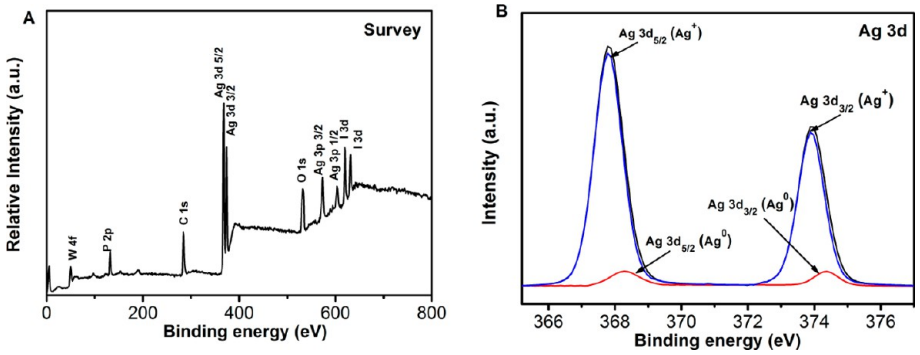

Figure 8. Survey (A) and Ag 3d (B) XPS spectra of the used Ag_3PO_4/AgI-20% sample.

Scheme 1. Photocatalytic Mechanism Scheme of Ag_3PO_4/AgI under Visible Light Irradiation (>420 nm)

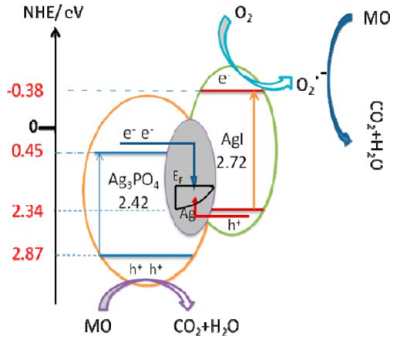

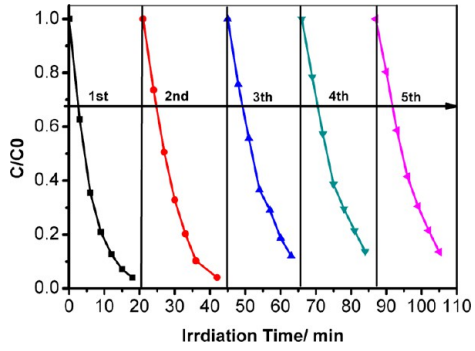

Figure 9. Cycle runs of Ag_3PO_4/AgI-20% for degradation of MO under visible light irradiation (>420 nm).

in the early stage of the PCO process and then act as the Z-scheme charge transmission bridge in the PCO process. The excellent photocatalytic activity of Ag_3PO_4/AgI may originate from the efficient separation of photogenerated electron−hole pairs through the Z-scheme system composed of Ag_3PO_4, Ag, and AgI. Moreover, Ag_3PO_4/AgI exhibited good stability in the PCO process under visible light irradiation. On the basis of their efficient and stable photocatalytic activity, Ag_3PO_4/AgI systems show promise for use in environmental purification of organic pollutants.

AUTHOR INFORMATION

Corresponding Author

*E-mail cexmfang@scut.edu.cn; Tel 86-20-87112997; Fax 86-20-87113870 (X.F.).

Notes

The authors declare no competing financial interest.

ACKNOWLEDGMENTS

This work was supported by the National Natural Science Foundation of China (No. 21276088).

REFERENCES

(1) Osterloh, F. E. Inorganic Nanostructures for Photoelectrochemical and Photocatalytic Water Splitting. *Chem. Soc. Rev.* **2013**, *42*, 2294−2320.

(2) Ibhadon, A. O.; Fitzpatrick, P. Heterogeneous Photocatalysis Recent Advances and Applications. *Catalysts* **2013**, *3*, 189−218.

(3) Fujishima, A.; Honda, K. Electrochemical Photolysis of Water at a Semiconductor Electrode. *Nature* **1972**, *238*, 37−8.

(4) Sayama, K.; Yoshida, R.; Kusama, H.; Okabe, K.; Abe, Y.; Arakawa, H. Photocatalytic Decomposition of Water into H_2 and O_2 by a Two-Step Photoexcitation Reaction Using a WO_3 Suspension Catalyst and an Fe^{3+}/Fe^{2+} Redox System. *Chem. Phys. Lett.* **1997**, *277*, 387−391.

(5) Kumar, S. G.; Devi, L. G. Review on Modified TiO_2 Photocatalysis under UV/Visible Light: Selected Results and Related Mechanisms on Interfacial Charge Carrier Transfer Dynamics. *J. Phys. Chem. A* **2011**, *115*, 13211−13241.

(6) Daghrir, R.; Drogui, P.; Robert, D. Modified TiO_2 for Environmental Photocatalytic Applications: A Review. *Ind. Eng. Chem. Res.* **2013**, *52*, 3581−3599.

(7) Wang, P.; Huang, B. B.; Qin, X. Y.; Zhang, X. Y.; Dai, Y.; Wei, J. Y.; Whangbo, M. H. Ag@AgCl: A Highly Efficient and Stable Photocatalyst Active under Visible Light. *Angew. Chem., Int. Ed.* **2008**, *47*, 7931−7933.

(8) Wang, P.; Huang, B. B.; Zhang, X. Y.; Qin, X. Y.; Jin, H.; Dai, Y.; Wang, Z. Y.; Wei, J. Y.; Zhan, J.; Wang, S. Y.; et al. Highly Efficient Visible-Light Plasmonic Photocatalyst Ag@AgBr. *Chem.—Eur. J.* **2009**, *15*, 1821−1824.

(9) Hu, C.; Peng, T. W.; Hu, X. X.; Nie, Y. L.; Zhou, X. F.; Qu, J. H.; He, H. Plasmon-Induced Photodegradation of Toxic Pollutants with Ag-AgI/Al_2O_3 under Visible-Light Irradiation. *J. Am. Chem. Soc.* **2010**, *132*, 857−862.

(10) Wang, X. F.; Li, S. F.; Yu, H. G.; Yu, J. G.; Liu, S. W. Ag_2O as a New Visible-Light Photocatalyst: Self-Stability and High Photocatalytic Activity. *Chem.—Eur. J.* **2011**, *17*, 7777−7780.

(11) Xu, C. W.; Liu, Y. Y.; Huang, B. B.; Li, H.; Qin, X. Y.; Zhang, X. Y.; Dai, Y. Preparation, Characterization, and Photocatalytic Properties of Silver Carbonate. *Appl. Surf. Sci.* **2011**, *257*, 8732−8736.

(12) Yi, Z. G.; Ye, J. H.; Kikugawa, N.; Kako, T.; Ouyang, S. X.; Stuart-Williams, H.; Yang, H.; Cao, J. Y.; Luo, W. J.; Li, Z. S.; et al. An Orthophosphate Semiconductor with Photooxidation Properties under Visible-Light Irradiation. *Nat. Mater.* **2010**, *9*, 559−564.

(13) Liu, J. J.; Fu, X. L.; Chen, S. F.; Zhu, Y. F. Electronic Structure and Optical Properties of Ag_3PO_4 Photocatalyst Calculated by Hybrid Density Functional Method. *Appl. Phys. Lett.* **2011**, *99*, 191903.

(14) Bi, Y.; Ouyang, S.; Umezawa, N.; Cao, J.; Ye, J. Facet Effect of Single-Crystalline Ag_3PO_4 Sub-Microcrystals on Photocatalytic Properties. *J. Am. Chem. Soc.* **2011**, *133*, 6490−6492.

(15) Bi, Y.; Hu, H.; Jiao, Z.; Yu, H.; Lu, G.; Ye, J. Two-Dimensional Dendritic Ag_3PO_4 Nanostructures and Their Photocatalytic Properties. *Phys. Chem. Chem. Phys.* **2012**, *14*, 14486−14488.
(16) Bi, Y.; Hu, H.; Ouyang, S.; Jiao, Z.; Lu, G.; Ye, J. Selective Growth of Metallic Ag Nanocrystals on Ag_3PO_4 Submicro-Cubes for Photocatalytic Applications. *Chem.—Eur. J.* **2012**, *18*, 14272−14275.
(17) Hu, H.; Jiao, Z.; Yu, H.; Lu, G.; Ye, J.; Bi, Y. Facile Synthesis of Tetrahedral Ag_3PO_4 Submicro-Crystals with Enhanced Photocatalytic Properties. *J. Mater. Chem. A* **2013**, *1*, 2387−2390.
(18) Jiao, Z.; Zhang, Y.; Yu, H.; Lu, G.; Ye, J.; Bi, Y. Concave Trisoctahedral Ag_3PO_4 Microcrystals with High-Index Facets and Enhanced Photocatalytic Properties. *Chem. Commun.* **2013**, *49*, 636−638.
(19) Wang, J.; Teng, F.; Chen, M.; Xu, J.; Song, Y.; Zhou, X. Facile Synthesis of Novel Ag_3PO_4 Tetrapods and the {110} Facets-Dominated Photocatalytic Activity. *CrystEngComm* **2013**, *15*, 39−42.
(20) Rawal, S. B.; Sung, S. D.; Lee, W. I. Novel Ag_3PO_4/TiO_2 Composites for Efficient Decomposition of Gaseous 2-Propanol under Visible-Light Irradiation. *Catal. Commun.* **2012**, *17*, 131−135.
(21) Liu, R.; Hu, P.; Chen, S. Photocatalytic Activity of Ag_3PO_4 Nanoparticle/TiO_2 Nanobelt Heterostructures. *Appl. Surf. Sci.* **2012**, *258*, 9805−9809.
(22) Yao, W.; Zhang, B.; Huang, C.; Ma, C.; Song, X.; Xu, Q. Synthesis and Characterization of High Efficiency and Stable Ag_3PO_4/TiO_2 Visible Light Photocatalyst for the Degradation of Methylene Blue and Rhodamine B Solutions. *J. Mater. Chem.* **2012**, *22*, 4050−4055.
(23) Zhang, L.; Zhang, H.; Huang, H.; Liu, Y.; Kang, Z. Ag_3PO_4/SnO_2 Semiconductor Nanocomposites with Enhanced Photocatalytic Activity and Stability. *New J. Chem.* **2012**, *36*, 1541−1544.
(24) Cao, B.; Dong, P.; Cao, S.; Wang, Y. BiOCl/Ag_3PO_4 Composites with Highly Enhanced Ultraviolet and Visible Light Photocatalytic Performances. *J. Am. Ceram. Soc.* **2013**, *96*, 544−548.
(25) Li, H.; Yin, S.; Wang, Y.; Sekino, T.; Lee, S. W.; Sato, T. Green Phosphorescence-Assisted Degradation of Rhodamine B Dyes by Ag_3PO_4. *J. Mater. Chem. A* **2013**, *1*, 1123−1126.
(26) Xu, Y. S.; Zhang, W. D. Monodispersed Ag_3PO_4 Nanocrystals Loaded on the Surface of Spherical Bi_2MoO_6 with Enhanced Photocatalytic Performance. *Dalton Trans.* **2013**, *42*, 1094−1101.
(27) Kumar, S.; Surendar, T.; Baruah, A.; Shanker, V. Synthesis of a Novel and Stable g-C_3N_4-Ag_3PO_4 Hybrid Nanocomposite Photocatalyst and Study of the Photocatalytic Activity under Visible Light Irradiation. *J. Mater. Chem. A* **2013**, *1*, 5333−5340.
(28) Liu, L.; Liu, J.; Sun, D. D. Graphene Oxide Enwrapped Ag_3PO_4 Composite: Towards a Highly Efficient and Stable Visible-Light-Induced Photocatalyst for Water Purification. *Catal. Sci. Technol.* **2012**, *2*, 2525−2532.
(29) Zhang, H.; Huang, H.; Ming, H.; Li, H.; Zhang, L.; Liu, Y.; Kang, Z. Carbon Quantum Dots/Ag_3PO_4 Complex Photocatalysts with Enhanced Photocatalytic Activity and Stability under Visible Light. *J. Mater. Chem.* **2012**, *22*, 10501−10506.
(30) Chen, G.; Sun, M.; Wei, Q.; Zhang, Y.; Zhu, B.; Du, B. Ag_3PO_4/Graphene-Oxide Composite with Remarkably Enhanced Visible-Light-Driven Photocatalytic Activity Toward Dyes in Water. *J. Hazard. Mater.* **2013**, *244*, 86−93.
(31) Yang, X.; Cui, H.; Li, Y.; Qin, J.; Zhang, R.; Tang, H. Fabrication of Ag_3PO_4-Graphene Composites with Highly Efficient and Stable Visible Light Photocatalytic Performance. *ACS Catal.* **2013**, *3*, 363−369.
(32) Dong, P.; Wang, Y.; Cao, B.; Xin, S.; Guo, L.; Zhang, J.; Li, F. Ag_3PO_4/Reduced Graphite Oxide Sheets Nanocomposites with Highly Enhanced Visible Light Photocatalytic Activity and Stability. *Appl. Catal., B* **2013**, *132*, 45−53.
(33) Bi, Y.; Ouyang, S.; Cao, J.; Ye, J. Facile Synthesis of Rhombic Dodecahedral AgX/Ag_3PO_4 (X = Cl, Br, I) Heterocrystals with Enhanced Photocatalytic Properties and Stabilities. *Phys. Chem. Chem. Phys.* **2011**, *13*, 10071−10075.
(34) Cao, J.; Luo, B. D.; Lin, H. L.; Xu, B. Y.; Chen, S. F. Visible Light Photocatalytic Activity Enhancement and Mechanism of AgBr/Ag_3PO_4 Hybrids for Degradation of Methyl Orange. *J. Hazard. Mater.* **2012**, *217*, 107−115.
(35) Lin, H. L.; Cao, J.; Luo, B. D.; Xu, B. Y.; Chen, S. F. Synthesis of Novel Z-Scheme AgI/Ag/AgBr Composite with Enhanced Visible Light Photocatalytic Activity. *Catal. Commun.* **2012**, *21*, 91−95.
(36) Zhang, H.; Wang, G.; Chen, D.; Lv, X.; Li, J. Tuning Photoelectrochemical Performances of Ag−TiO_2 Nanocomposites via Reduction/Oxidation of Ag. *Chem. Mater.* **2008**, *20*, 6543−6549.